PANoptosis-like cell death in ischemia/reperfusion injury of retinal neurons

Wei-Tao Yan[1, #], Wen-Juan Zhao[1, #], Xi-Min Hu[2], Xiao-Xia Ban[1], Wen-Ya Ning[3], Hao Wan[1], Qi Zhang[1, *], Kun Xiong[1, 4, 5 *]

See related Commentaries, pp 339–343

https://doi.org/10.4103/1673-5374.346545

Date of submission: November 28, 2021

Date of decision: December 20, 2021

Date of acceptance: April 11, 2022

Date of web publication: July 1, 2022

From the Contents

Graphical Abstract

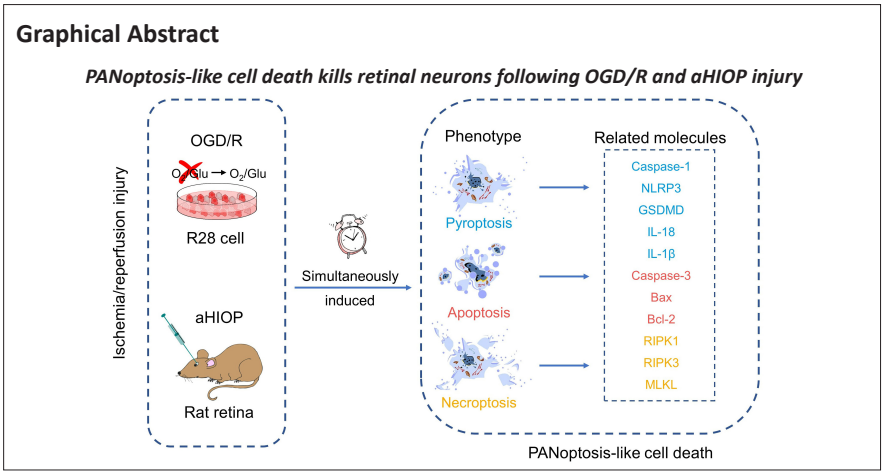

Abstract

PANoptosis is a newly identified type of regulated cell death that consists of pyroptosis, apoptosis, and necroptosis, which simultaneously occur during the pathophysiological process of infectious and inflammatory diseases. Although our previous literature mining study suggested that PANoptosis might occur in neuronal ischemia/reperfusion injury, little experimental research has been reported on the existence of PANoptosis. In this study, we used *in vivo* and *in vitro* retinal neuronal models of ischemia/reperfusion injury to investigate whether PANoptosis-like cell death (simultaneous occurrence of pyroptosis, apoptosis, and necroptosis) exists in retinal neuronal ischemia/reperfusion injury. Our results showed that ischemia/reperfusion injury induced changes in morphological features and protein levels that indicate PANoptosis-like cell death in retinal neurons both *in vitro* and *in vivo*. Ischemia/reperfusion injury also significantly upregulated caspase-1, caspase-8, and NLRP3 expression, which are important components of the PANoptosome. These results indicate the existence of PANoptosis-like cell death in ischemia/reperfusion injury of retinal neurons and provide preliminary experimental evidence for future study of this new type of regulated cell death.

Key Words: apoptosis; gasdermin-D (GSDMD); ischemia/reperfusion; mixed lineage kinase domain-like protein (MLKL); necroptosis; NOD-like receptor protein 3 (NLRP3); PANoptosis; pyroptosis; receptor-interacting protein kinase 3 (RIPK3); retinal neuron

Introduction

PANoptosis is a phenomenon in which pyroptosis, apoptosis, and necroptosis simultaneously occur during the pathophysiological process of some diseases, and they can be regulated at the same time (Malireddi et al., 2019). A series of studies have reported that PANoptosis is regulated by the PANoptosome complex, which is assembled by some key regulators of pyroptosis, apoptosis, and necroptosis (Malireddi et al., 2019, 2020; Banoth et al., 2020; Christgen et al., 2020; Samir et al., 2020). The protein complex simultaneously regulates pyroptosis, apoptosis, and necroptosis (Christgen et al., 2020; Samir et al., 2020). In addition to infectious diseases, many other diseases, such as nervous system diseases, involve cell death and immune response, and there are many studies on the regulated cell deaths (RCDs) pyroptosis, apoptosis, and necroptosis (Yuan and Yankner, 2000; Elmore, 2007; Tan et al., 2014; Ofengeim et al., 2015; Kesavardhana and Kanneganti, 2017; Ge et al., 2018; Yuan et al., 2019; Guo et al., 2020; Liao et al., 2021; Yan et al., 2021). These RCDs have been shown to be associated with immune response (Semmler et al., 2005; Takeda et al., 2008; Basuroy et al., 2009; Huang et al., 2018; Liu et al., 2019b; Wang et al., 2019a; Zhou et al., 2019; Chen et al., 2021; McKenzie et al., 2020; Hu et al., 2021; Wu et al., 2021). These studies indicated the possibility that PANoptosis plays a larger role in the nervous system. Thus, we conducted a literature mining study to explore this hypothesis (Yan et al., 2022). In that study, we found that under experimental conditions, the three RCD forms of PANoptosis exist in models of middle cerebral artery occlusion and oxygen-glucose deprivation/recovery (OGD/R). To validate the hypothesis that PANoptosis exists in retinal ischemia/reperfusion (I/R) injury, the present study used both *in vitro* and *in vivo* I/R models (OGD/R and acute high intraocular pressure [aHIOP]) of retinal neurons to investigate the existence of PANoptosis-like cell death under experimental conditions.

Methods

Animals and aHIOP model

The animals used in the experiment were male Sprague-Dawley rats (n = 90) with a weight range of 250–300 g and an age of 8 weeks. The experiments were approved by the Animal Ethics Committee of Basic Medical School of Central South University on March 2, 2021 (approval No. 2021-XMSB-0002). The animals were purchased from the Hunan STJ Laboratory Animal Co., Ltd (Hunan, China) (license No. SCXK (Xiang) 2019-0004), and the experimental protocols and operating procedures were in accordance with the Guidelines for Animal Experiments of Central South University under the Law of Animal Protection and Management of the Chinese Government. Rats were randomly divided into three groups using a random number table: Sham, aHIOP, and aHIOP + inhibitor (n = 30 rats/group).

[1]Department of Human Anatomy and Neurobiology, School of Basic Medical Science, Central South University, Changsha, Hunan Province, China; [2]Department of Dermatology, Xiangya Hospital, Central South University, Changsha, Hunan Province, China; [3]Department of Human Resources, Third Xiangya Hospital of Central South University, Changsha, Hunan Province, China; [4]Hunan Key Laboratory of Ophthalmology, Changsha, Hunan Province, China; [5]Key Laboratory of Emergency and Trauma, Ministry of Education, College of Emergency and Trauma, Hainan Medical University, Haikou, Hainan Province, China

*Correspondence to: Kun Xiong, MD, xiongkun2001@163.com; Qi Zhang, MD, zhangqi2014@csu.edu.cn.

https://orcid.org/0000-0002-3103-6028 (Kun Xiong); https://orcid.org/0000-0001-6300-6491 (Qi Zhang); https://orcid.org/0000-0002-2561-9673 (Wei-Tao Yan); https://orcid.org/0000-0002-3616-5347 (Wen-Juan Zhao)

#These two authors contributed equally to this paper.

Funding: *The study was supported by the National Natural Science Foundation of China, Nos. 81772134, 81971891, 82172196, 81571939 (all to KX); the Key Laboratory of Emergency and Trauma (Hainan Medical University) of Ministry of Education, No. KLET-202108 (to KX); the Fundamental Research Funds for the Central Universities of Central South University of China, No. 2020zzts218 (to WTY); Hunan Provincial Innovation Foundation for Postgraduate of China, No. CX20200116 (to WTY).*

How to cite this article: *Yan WT, Zhao WJ, Hu XM, Ban XX, Ning WY, Wan H, Zhang Q, Xiong K (2023) PANoptosis-like cell death in ischemia/reperfusion injury of retinal neurons. Neural Regen Res 18(2):357-363.*

An aHIOP model was prepared using previously reported methods (Rosenbaum et al., 1998, 2001; Huang et al., 2013; Wang et al., 2020). Sprague-Dawley rats were intraperitoneally injected with 2% pentobarbital sodium (40 mg/kg; FWD Chem Co., Shanghai, China) to ensure that the animals were generally anesthetized. A sterilized 30-gauge needle was inserted into the anterior chamber of one randomly selected eye (this eye was then referred to as the ocular hypertension [OHT] eye) of the rats, and normal saline (NS) was injected into the anterior chamber through an intravenous tube to generate artificial intraocular pressure (IOP).

IOP was slowly increased to 110 mmHg and maintained for 60 minutes by adjusting the NS volume based on the IOP, which was measured with the hand-held tonometer Tono-Pen XL (Medtronic Inc., Jacksonville, FL, USA). Then, IOP was gradually returned to normal level and maintained for 48 hours before retinal tissue collection. In the Sham group, a sterilized 30-gauge needle was inserted into the anterior chamber of the eyes without elevating the IOP. Specific inhibitors for RCDs were used *in vivo* as follows: the inhibitor was dissolved in NS, and the inhibitor solution (or dimethyl sulfoxide [DMSO] for control) was injected into the vitreous cavity 30 minutes before treatment with high IOP.

After the aHIOP model was completed, the rats were sacrificed quickly, and their eyeballs were removed and fixed in 4% paraformaldehyde at 4°C for 24 hours. Then they were treated with 15% and 30% sucrose solution sequentially for dehydration. After dehydration, the eyeball was dissected, the cornea, lens and vitreous body were removed, and the retinal tissue was retained. The retina was embedded with OCT glue (Sakura Finetek, Tokyo, Japan) and frozen at –80°C for 24 hours. Frozen sections were cut to a thickness of 20 μm using a cryotome (Cryotome FSE, Thermo Electron Corporation, Waltham, MA, USA). The sections were stored at –20°C until use. All animal experiments were conducted independently at least five times.

Cell cultures

R28 cells (retinal precursor cells) were provided by Dr. Lei Shang (Jiang Xi Research Institute of Ophthalmology and Visual Sciences, Affiliated Eye Hospital of Nanchang University, Jiangxi, China) as a gift. This R28 cell line has been tested by short tandem repeats (STR) analysis and it is not misidentified or contaminated according to current database and widely used in our previous studies (Rong et al., 2020; Wang et al., 2020; Huang et al., 2021). R28 cells were cultured in low glucose Dulbecco's modified Eagle's medium (DMEM; low glucose: 1000 mg/L glucose; Cat# MA0580, Meilunbio, Dalian, Liaoning, China) supplemented with 10% fetal bovine serum (FBS; Hyclone, Cat# SV30087GE Healthcare Life Sciences, Logan, UT, USA) and 1% penicillin/streptomycin (PS; 10,000 U/mL penicillin, 10,000 μg/mL streptomycin in 0.85% NaCl; Thermo Fisher Scientific, Waltham, MA, USA, Cat# SV30010) at 37°C in a 5% CO_2 cell culture incubator (Thermo Scientific Forma Series 3111, Thermo Fisher Scientific). R28 cells were subcultured every 2 or 3 days. The R28 cells were used for related experiments after drug treatment.

OGD/R injury of R28 cells *in vitro*

The OGD/R model was used to simulate I/R injury *in vitro* (Hu et al., 2020b; Xie et al., 2020). When R28 cells were subcultured to the 3rd generation and had grown to about 80% density, the OGD/R model was performed on the cells using a protocol based on published literature (Wang et al., 2018b, 2020; Huang et al., 2021). When the R28 cells were cultured to a suitable state, the initial culture medium (low glucose DMEM with 10% FBS and 1% PS) was replaced with glucose-free medium (DMEM, no glucose, Thermo Fisher Scientific, Cat# 1966025) with FBS and PS. After the medium was changed, cell culture containers were placed in the OGD treatment device, which maintained a hypoxic condition (O_2 < 1%). This device was made by our research team, and contained an airtight box, oxygen concentration sensor, and a hypoxic air supply pipeline (95% nitrogen and 5% CO_2) to replace the oxygen containing air. It was well-tested and applied in our previous studies (Chen et al., 2016; Wang et al., 2018, 2020; Huang et al., 2021). The R28 cells subjected to OGD treatment were cultured at 37°C for 2 hours. After OGD injury, the cells were returned to the initial culture condition (low glucose DMEM with 10% FBS and 1% PS at 37°C in a 5% CO_2 cell culture incubator) for 2 hours. The normal control group was maintained in the normal culture medium (low glucose DMEM with 10% FBS and 1% PS) in a culture incubator (Thermo Scientific Forma Series 3111, Thermo Fisher Scientific) at 37°C and 5% CO_2 for the same length of time. All cell experiments were performed at least three times independently.

Drug treatments

Z-VAD-FMK (Z-VAD; Cat# S7023, Selleck Chemicals, Houston, TX, USA) was dissolved in DMSO at a final concentration of 50 μM. Disulfiram (DSF; Selleck Chemicals, Cat# S1680) was dissolved in DMSO at a final concentration of 0.3 μM. Necrostatin-1 (Nec-1; Cat# S8037, Selleck Chemicals) was dissolved in DMSO at a final concentration of 20 μM. R28 cells were pretreated with drugs (or DMSO for control) for 1 hour before OGD modeling (Wang et al., 2018, 2020; Huang et al., 2021). For treatment with a combination of these inhibitors in the OGD/R model, the final concentration of each inhibitor in combination was the same as that of a single inhibitor mentioned above. In the aHIOP model, the amounts of Z-VAD (10 mM), DSF (10 mM), and Nec-1 (20 mM) injected into the OHT eye were 3, 0.5 and 1.5 μL, respectively. The processing time was 30 minutes.

Propidium iodide staining

Propidium iodide (PI; MilliporeSigma, Burlington, MA, USA, Cat# P4170) staining combined with Nec-1 was used to indicate necroptosis. Nec-1 is a specific inhibitor of necroptosis that targets receptor-interacting protein kinase 1 (RIPK1), which is the key upstream kinase of necroptosis activation (Degterev et al., 2008). PI is a nuclear dye that fluoresces red when it binds to DNA. When the membrane integrity is damaged by cell necrosis, PI can enter the cell and bind to DNA, so it is usually used to detect necrotic cells (Nicoletti et al., 1991; Riccardi and Nicoletti, 2006). PI was dissolved in 0.01 M phosphate buffered saline (PBS) at a final concentration of 10 μg/mL (Wang et al., 2018, 2020; Huang et al., 2021). After OGD/R and drug treatment, R28 cells were gently washed three times with PBS for 5 minutes each, stained with PI dye, and placed in the cell culture incubator (Thermo Scientific Forma Series 3111, Thermo Fisher Scientific) at room temperature (25°C) for 20 minutes while being protected from light. After removal of PI dye, R28 cells were gently washed with PBS three times for 5 minutes each, fixed with 4% paraformaldehyde (Solarbio, Beijing, China, Cat# P1110) at room temperature (25°C) for 20 minutes, and washed gently with PBS three times for 5 minutes each. In the rat aHIOP groups, 5 μL of PI (100 μg/mL) was injected through the anterior chamber angle into the intravitreal space of the OHT eye 30 minutes before the animals were killed. The R28 cells and sections stained with PI were subsequently stained using Hoechst 33258 (MilliporeSigma, Cat# 94403) in 0.01 M PBS at a final concentration of 0.5 μg/mL for 10 minutes at room temperature, and then the cells were washed with PBS three times for 5 minutes each.

The cells were covered with a mixture of glycerol and PBS at a ratio of 1:9 and observed under a fluorescence microscope (Olympus, Tokyo, Japan) (Wang et al., 2018, 2020; Huang et al., 2021). Images were taken at six random positions for each sample. The percentage of PI-positive cells was analyzed by ImageJ v.1.4.3 software (NIH, Baltimore, MD, USA).

Terminal deoxynucleotidyl transferase-mediated nick end labeling

Terminal deoxynucleotidyl transferase-mediated nick end labeling (TUNEL) Apoptosis Detection Kit combined with Z-VAD was used to detect apoptosis of R28 cells (green fluorescent, Meilunbio, Cat# MA0223) and in animal tissue (red fluorescent, Meilunbio, Cat# MA0224). Z-VAD is an inhibitor that can cross the cell membrane and target cysteine aspartate-specific proteases (caspase) to irreversibly inhibit caspase activation and thus block apoptosis in cells (Slee et al., 1996; Shimizu and Pommier, 1997; Van Noorden, 2001). TUNEL is a common method to detect cell apoptosis; when apoptosis occurs, DNA breaks to produce the 3'-OH terminals, and TUNEL labels 3'-OH terminals with fluorescein to stain apoptotic cells (Quigley et al., 1995; Saraste and Pulkki, 2000). After OGD/R and drug treatment, R28 cells were fixed with 4% paraformaldehyde at room temperature for 30 minutes, followed by PBS containing proteinase K (20 μg/mL; Meilunbio, Cat# MA0224-2) at room temperature for 5 minutes. Rat retinal sections were washed with PBS three times for 5 minutes each, followed by washes with PBS containing proteinase K (20 μg/mL) at 37°C for 20 minutes. After the TdT reaction solution was prepared according to the kit protocol, reaction solution was added to the washed cells and sections, and the cells were treated at 37°C for 2 hours in the dark. Subsequently, the cells and sections were washed with PBS three times for 5 minutes each, and then stained with Hoechst 33258 (see Section "Propidium iodide staining"). After three washes with PBS for 5 minutes each, the cells were observed under a fluorescence microscope (Olympus). Images were taken at six random positions for each sample. The percentage of TUNEL-positive cells was analyzed by Image J software.

Ethidium Homodimer III staining

Ethidium Homodimer III (EthD-III; Biotium, Fremont, CA, USA, Cat# 40050) staining combined with DSF was used to indicate pyroptosis. DSF inhibits GSDMD expression and interferes with pore formation triggered by GSDMD in the cell membrane to prevent the release of interleukin and other inflammatory factors (Zhang et al., 2021a, b). This special function enables DSF to inhibit cell pyroptosis (Hu et al., 2020a). EthD-III is a fluorescent nucleic acid dye that cannot pass through normal cell membranes. It selectively stains dead cells with damaged cell membranes, and is a useful dye for pyroptosis (Pan et al., 2018; Wang et al., 2019b). EthD-III was dissolved in 1 × PBS and the solution concentration was adjusted to 1 μg/mL. R28 cells were treated with EthD-III solution for 10 minutes at room temperature, followed by three PBS washes for 5 minutes each. Subsequently, they were soaked with 4% paraformaldehyde for 20 minutes, followed by three PBS washes for 5 minutes each. Then, 5 μL of EthD-III (100 μg/mL) was injected into the intravitreal space of the eye 30 minutes before the animals were killed. Cells and sections stained with EthD-III were stained using Hoechst 33258 (MilliporeSigma, Cat# 94403) (see Section "Propidium iodide staining"). The cells were observed under a fluorescence microscope. Images were taken at six random positions for each sample. The percentage of EthD-III-positive cells was analyzed by Image J software.

Western blot assay

R28 cells were lysed in ice-cold RIPA buffer (CWBIO, Beijing, China) with 1% protease inhibitors (CWBIO) and 1% phosphatase inhibitors (CWBIO). Protein concentrations were determined with the BCA protein assay kit (CWBIO). Protein samples were separated by 10% or 12% sodium dodecyl sulfate polyacrylamide gel and transferred to nitrocellulose membranes (Pall, New York, NY, USA, Cat# 66485). The membranes were incubated at room temperature for 2 hours in 5% nonfat dry milk, and then incubated with primary antibodies overnight at 4°C. The reactions were followed by incubation with peroxidase-labeled secondary antibodies. Primary antibodies were: anti-BAX (1:1000, Proteintech, Rosemont, IL, USA, Cat# 50599-2-Ig, RRID: AB_2061561), anti-BCL-2 (1:2000, Proteintech, Cat# 26593-1-AP, RRID:

AB_2818996), anti-caspase 1 (1:500, Proteintech, Cat# 22915-1-AP, RRID: AB_2876874), anti-caspase 3 (1:500, Proteintech, Cat# 19677-1-AP, RRID: AB_10733244), anti-gasdermin-D (GSDMD; 1:1000, Proteintech, Cat# 20770-1-AP, RRID: AB_10696319), anti-interleukin-1β (IL-1β; 1:1000, Bioss, Beijing, China, Cat# bs-0812R, RRID: AB_10855142), anti-IL-18 (1:1000, Proteintech, Cat# 10663-1-AP, RRID: AB_2123636), anti-mixed lineage kinase domain-like protein (MLKL; 1:1000, ABclonal, Cat# A13451, RRID: AB_2861686), anti-NOD-like receptor protein 3 (NLRP3; 1:1000, Abcam, Cambridge, UK, Cat# 263899, RRID: AB_2889890), anti-RIPK3 (1:1000, Novus, Shanghai, China, Cat# NBP1-77299, RRID: AB_11040928), and anti-β-Actin (1:4000, Affinity Biosciences, Changzhou, Guangdong Province, China, Cat# AF7018, RRID: AB_2839420). The secondary antibodies were peroxidase-conjugated affiniPure donkey anti-rabbit IgG (1:5000, Jackson Immuno Research, West Grove, PA, USA, Cat# 711-035-152, RRID: AB_10015282) and donkey anti-mouse IgG (H+L, 1:5000, Jackson Immuno Research, Cat# 715-035-150, RRID: AB_2340770). The membranes were developed with electrochemiluminescent reagents and the band intensities were quantitated with Image J software. The level of expression was normalized to the level of β-actin. All cell experiments were performed at least three times independently.

Enzyme-linked immunosorbent assay

The expression levels of IL-1β and IL-18 in R28 cell culture supernatant were determined by enzyme-linked immunosorbent assay (ELISA) kits (rat IL-1β, F2923-A; rat IL-18, F3070-A; KX-Bio Co., Shanghai, China). Following OGD/R treatment, cell culture supernatants were collected and centrifuged at 3000 r/min for 20 minutes. Then IL-1β and IL-18 concentrations were determined according to the manufacturer's instructions.

Immunofluorescence staining

Frozen sections of rat retinal tissue were placed at room temperature for 30 minutes, washed three times with PBS for 5 minutes each, sealed with 1 × PBS containing 5% bovine serum albumin and 0.3% Triton X-100 for 2 hours, and incubated with primary antibodies overnight at 4 °C. Primary antibodies were: anti-cleaved caspase 3 (1:50, Cell Signaling Technology, Oslo, Norway, Cat# 9664, RRID: AB_2070042), anti-GSDMD (1:50; Proteintech, Cat# 20770-1-AP, RRID: AB_10696319), anti-MLKL (1:50; ABclonal, Cat# A13451, RRID: AB_2861686), and anti-NeuN (1:2000, Millipore, Darmstadt, Germany, Cat# MAB377, RRID: AB_2298772). After three PBS washes for 5 minutes each, the sections were incubated with fluorescently labeled secondary antibody at room temperature for 2 hours in the dark. After three PBS washes for 5 minutes each, the sections were stained using Hoechst 33258 (Cat# 94403, MilliporeSigma) (see Section "Propidium iodide staining"). After three PBS washes for 5 minutes each, anti-fluorescence quenching agent was dropped on the sections, and the tissues were covered with glycerin and cover glass. Finally, images were captured using a fluorescence microscope and analyzed by ImageJ software. All animal experiments were performed at least five times independently.

Statistical analysis

Data were summarized as the mean ± standard deviation of independent replicates. The significance of differences between two groups was determined by two-tailed Student's *t*-test using GraphPad Prism 8 software (GraphPad Software Inc., San Diego, CA, USA, www.graphpad.com). $P < 0.05$ was considered statistically significant.

Results

OGD/R induces morphological changes of PANoptosis-like cell death in R28 cells

We first investigated whether OGD/R simultaneously induces the morphological changes of PANoptosis-like cell death in R28 cells (**Figure 1**). The OGD/R treatment and staining timeline were the same in each group. Cell staining results indicated that the OGD/R treatment significantly induced apoptosis (TUNEL staining; **Figure 2A** and **D**), pyroptosis (EthD-III staining; **Figure 2B** and **D**), and necroptosis (PI staining; **Figure 2C** and **D**). The RCD morphology of cells treated with OGD/R after pretreatment with inhibitors of apoptosis (Z-VAD; **Figure 2A** and **D**), pyroptosis (DSF; **Figure 2B** and **D**), and necroptosis (Nec-1; **Figure 2C** and **D**) was significantly reversed. These results indicated that PANoptosis-like cell death occurred in R28 cells following OGD/R injury, which is similar to those observed in PANoptosis in other models (Kuriakose and Kanneganti, 2019; Malireddi et al., 2019; Karki et al., 2021).

OGD/R induces expression changes of key proteins in PANoptosis-like cell death in R28 cells

The above results indicated that PANoptosis-like cell death occurred at the morphological level, thus it was important to next determine the expression changes of hallmark proteins for apoptosis, pyroptosis, and necroptosis in R28 cells following OGD/R injury. As shown in **Figure 3A**, western blot assay showed that OGD/R treatment caused a significant increase of cleaved caspase-3 compared with the control and caspase inhibitor (Z-VAD) groups. The results also showed that compared with the control and Z-VAD groups, OGD/R treatment significantly increased the expression of pro-apoptotic protein BAX and decreased the expression of anti-apoptotic protein BCL-2.

Western blot showed that OGD/R treatment increased expression of NLRP3 and cleaved caspase-1 (CASP1 p20) (**Figure 3B**), key proteins in the pyroptosis pathway. Expression of cleaved GSDMD and GSDMD-N (p30), a driver of pyroptosis, were also upregulated by the OGD/R treatment. Elevated expression of proinflammatory cytokines IL-1β (p17) and IL-18 (p22) were also observed in the OGD/R group. These expression changes were reversed

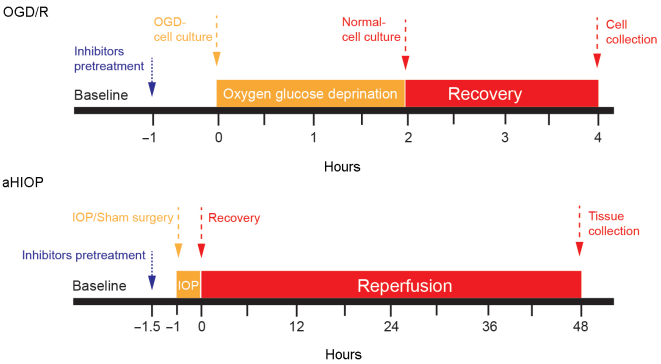

Figure 1 | **Schematic of the experimental timeline of OGD/R and aHIOP modeling.** In the OGD/R model (top panel), R28 cells were pretreated with inhibitors (or DMSO for control) for 1 hour before establishing the OGD model. Then, the initial culture medium was replaced with glucose-free medium. The cell culture containers were placed in the OGD treatment device, which maintained a hypoxic condition (O_2 < 1%). OGD treatment lasted for 2 hours. After OGD treatment, the cells were returned to the initial culture condition for 2 hours. The normal control group was maintained in the normal culture condition for the same length of time. In the aHIOP model (bottom panel), inhibitors (or DMSO for control) were injected into the vitreous cavity 30 minutes before HIOP/sham surgery. To induce ocular hypertension, normal saline was injected into the anterior chamber to form artificial intraocular pressure (IOP). IOP was slowly increased to 110 mmHg and maintained for 60 minutes, then gradually returned to normal level and maintained for 48 hours before retinal tissue collection. In the sham group, a sterilized needle was inserted into the anterior chamber without elevating the IOP at the same time point. aHIOP: Acute high intraocular pressure; DMSO: dimethyl sulphoxide; OGD/R: oxygen-glucose deprivation/recovery.

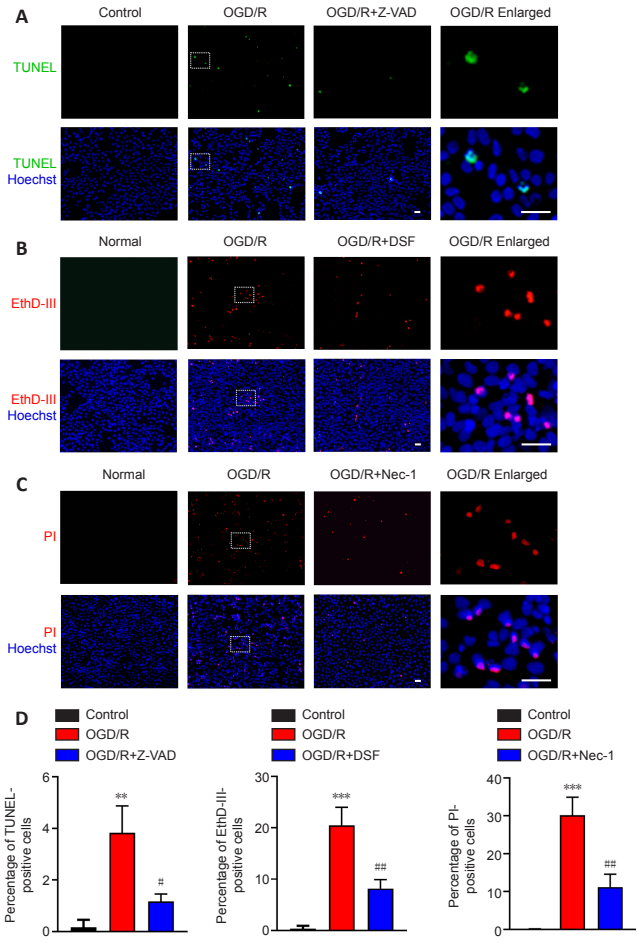

Figure 2 | **OGD/R-induced R28 cells exhibit pyroptosis, apoptosis, and necroptosis.** (A) Terminal-deoxynucleotidyl transferase mediated nick end labeling (TUNEL) staining for R28 cells. R28 cells were treated with OGD/R and Z-VAD. (B) Ethidium Homodimer III (EthD-III) staining for R28 cells. R28 cells were treated with OGD/R and DSF. (C) Propidium iodide (PI) staining for R28 cells. R28 cells were treated with OGD/R and Nec-1. Scale bars: 50 μm. (D) Percentage of TUNEL-, EthD-III-, PI-positive cells (mean ± SD, $n = 3$). $^{**}P < 0.01$, $^{***}P < 0.001$, *vs.* Control; $^{\#}P < 0.05$, $^{\#\#}P < 0.01$, *vs.* OGD/R (Student's *t*-test). All cell experiments were performed at least three times independently. DSF: Disulfiram; Nec-1: necrostatin-1; OGD/R: oxygen-glucose deprivation/recovery; Z-VAD: Z-VAD-FMK.

by the specific GSDMD inhibitor DSF. Moreover, the ELISA assay indicated that expressions of mature IL-1β and IL-18 were significantly increased in the R28 cell culture supernatant after OGD/R treatment, and these increases were reversed by DSF inhibitor (**Figure 3D**). The above results indicated caspase-1/NLRP3/GSDMD-mediated pyroptosis in R28 cells following OGD/R treatment.

Increases in the protein levels of phosphorylated RIPK3 and phosphorylated MLKL are hallmarks of necroptosis (Vandenabeele et al., 2010; Pasparakis and Vandenabeele, 2015). As depicted in **Figure 3C**, the OGD/R treatment remarkably upregulated the expressions of phosphorylated RIPK3 and phosphorylated MLKL, and inhibitors of necroptosis prevented this increase. Taken together, these results indicated that OGD/R treatment induced pyroptosis, apoptosis and necroptosis in R28 cells at the protein level at the same time point, and further suggest the existence of PANoptosis-like cell death in R28 cells.

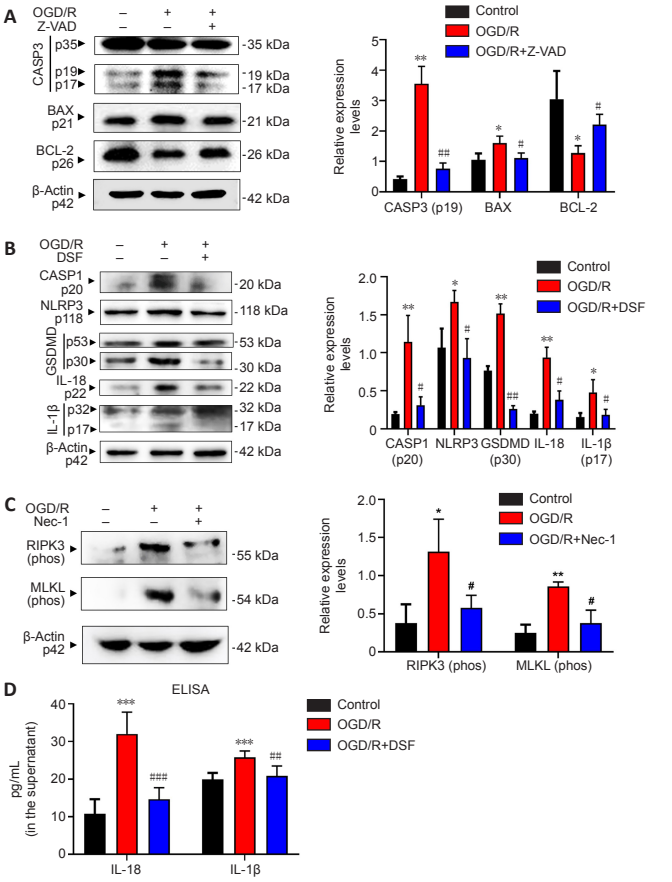

Figure 3 | Treatment with OGD/R upregulates key proteins of pyroptosis, apoptosis and necroptosis in R28 cells.

(A) Western blotting of caspase-3, BAX and Bcl-2 in R28 cells after treatment with OGD/R and Z-VAD inhibitor. (B) Western blotting of caspase-1, NLRP3, GSDMD, IL-18, IL-1β in R28 cells after treatment with OGD/R and DSF inhibitor. (C) Western blotting of phosphorylated RIPK3 and phosphorylated MLKL in R28 cells after treatment with OGD/R and Nec-1 inhibitor. Quantifications of protein expression are shown to the right of each western blot image. (D) ELISA of the expressions of mature IL-1β and IL-18 in the R28 cell culture supernatant after treatment with OGD/R and DSF inhibitor. Data are expressed as the mean ± SD (n = 3). *P < 0.05, **P < 0.01 *vs.* Control; #P < 0.05, ##P < 0.01, *vs.* OGD/R (Student's *t*-test). All cell experiments were performed at least three times independently. BAX: Bcl-2-associated X protein; CASP: caspase; DSF: disulfiram; GSDMD: Gasdermin-D; IL: interleukin; MLKL: mixed lineage kinase domain-like; Nec-1: necrostatin-1; NLRP3: NACHT, LRR, and PYD domains-containing protein 3; OGD/R: oxygen-glucose deprivation/recovery; RIPK: receptor-interacting protein kinase; Z-VAD: Z-VAD-FMK.

Combination of three RCD inhibitors significantly protects R28 cells following OGD/R

The results above indicated that OGD/R treatment induced PANoptosis-like cell death in R28 cells at the same time point. Next, we investigated whether the cell loss following OGD/R treatment is mainly dependent on this kind of combined cell death. Thus, pretreatment with different combinations of inhibitors for apoptosis, pyroptosis, and necroptosis was used to assess the protective effects on cell loss against OGD/R treatment. As shown in **Figure 4A** and **B**, Z-VAD combined with either DSF or Nec-1 had a better protective effect than that of Z-VAD alone, as measured by TUNEL-positive cell death, following OGD/R treatment. There was no significant difference between the triple combination and the double combinations, and the TUNEL-positive cell death was largely reversed by the combined pretreatments. The combination of DSF with Z-VAD, or with both Z-VAD and Nec-1, had a better protective effect on EthD-III-positive cell death than DSF alone (**Figure 5A** and **B**). The triple

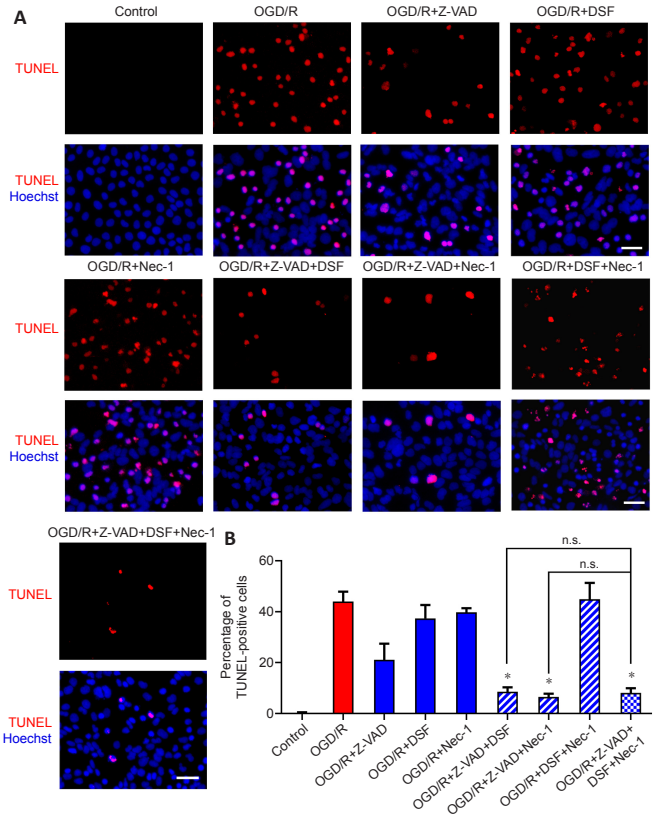

Figure 4 | Combination of RCD inhibitors decreases the OGD/R-induced TUNEL-positive cells.

(A) TUNEL staining for R28 cells treated with combinations of RCD inhibitors following OGD/R treatment. Scale bars: 50 μm. Red: TUNEL-positive cells. (B) Percentage of TUNEL-positive cells (mean ± SD, n = 3). *P < 0.05, *vs.* OGD/R + Z-VAD (Student's *t*-test). DSF: Disulfiram; n.s.: not significant; Nec-1: necrostatin-1; OGD/R: oxygen-glucose deprivation/recovery; RCD: regulated cell death; TUNEL: terminal-deoxynucleotidyl transferase mediated nick end labeling; Z-VAD: Z-VAD-FMK.

combination of DSF, Z-VAD and Nec-1 had the largest protective effect on EthD-III-positive cell death compared with each of the double combinations. PI staining also indicated that the combination of Nec-1 with Z-VAD, or with both Z-VAD and DSF, had a larger protective effect than Nec-1 alone (**Figure 6A** and **B**). Moreover, the triple combination of Nec-1, Z-VAD and DSF had a larger protective effect on PI-positive cell death than the double combination of Nec-1 and DSF. Taken together, these results suggested that OGD/R-induced R28 cell death is mainly driven by PANoptosis-like cell death.

An aHIOP model induces PANoptosis-like cell death *in vivo*

The above experiments indicated that OGD/R injury can induce PANoptosis-like cell death *in vitro*. Next, we used a rat aHIOP model to investigate whether I/R injury can induce PANoptosis-like cell death *in vivo* (**Figure 1**). As shown in **Figure 7A**, aHIOP treatment induced apoptotic cell death of retinal neurons (indicated by TUNEL staining) in the ganglion cell layer (GCL), inner nuclear layer (INL), and outer nuclear layer (ONL). The increased TUNEL staining was significantly reduced by Z-VAD pretreatment. Increased caspase-3 expression was detected by immunofluorescence staining in retinal neurons, which further indicated the occurrence of apoptosis in retinal neurons following aHIOP treatment (**Figure 8A**). Furthermore, the co-immunofluorescence staining of caspase-3 and NeuN indicated that caspase-3 was activated in the retinal ganglion cells (RGCs) of aHIOP-treated retina.

The existence of pyroptosis in retinal neurons was indicated by EthD-III-positive staining in GCL and INL of aHIOP-treated retina (**Figure 7B**). EthD-III-positive staining in the retina was significantly reduced by pretreatment of specific pyroptosis inhibitor DSF. Moreover, as shown in **Figure 8B**, aHIOP treatment significantly increased GSDMD expression (indicated by immunofluorescence staining) in the GCL and INL, which was consistent with the EthD-III staining. Also, the co-immunofluorescence staining of GSDMD and NeuN indicated the activation of GSDMD in RGCs. Thus, these results indicated that aHIOP treatment induced pyroptosis in retinal neurons *in vivo*.

Similarly, aHIOP treatment increased PI staining, suggesting that aHIOP treatment induced necroptotic cell death, in the GCL, INL, and ONL of the retina, and Nec-1 pretreatment significantly reduced the PI-positive staining (**Figure 7C**). Furthermore, after aHIOP treatment, immunofluorescence staining showed increased expression of MLKL, a key protein of necroptosis execution, indicating that aHIOP treatment induced retinal cell necroptosis (**Figure 8C**). The co-immunofluorescence staining of MLKL and NeuN indicated the activation of MLKL in RGCs of aHIOP-treated retina. Taken together, the results demonstrated that PANoptosis-like cell death occurred *in vivo* in retinal neurons following aHIOP injury.

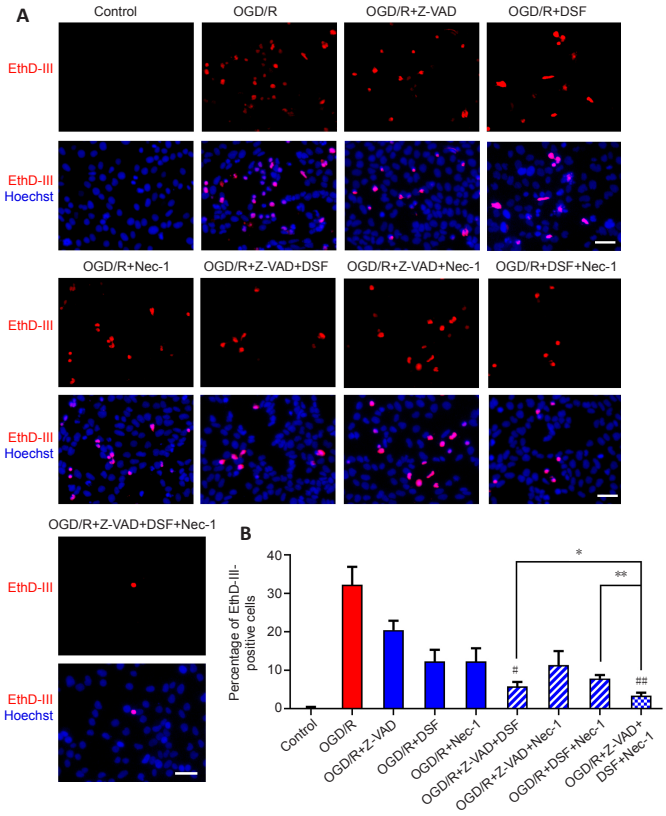

Figure 5 | Combination of RCD inhibitors decreases the OGD/R-induced EthD-III-positive cells.
(A) EthD-III staining for R28 cells treated with combinations of RCD inhibitors following OGD/R treatment. Red: EthD-III-positive cells. Scale bars: 50 μm. (B) Percentage of EthD-III-positive cells (mean ± SD, n = 3). *P < 0.05, **P < 0.01, *vs.* OGD/R + Z-VAD + DSF + Nec-1; #P < 0.05, ##P < 0.01, *vs.* OGD/R + DSF (Student's t-test). DSF: Disulfiram; EthD-III: Ethidium Homodimer III; Nec-1: necrostatin-1; OGD/R: oxygen-glucose deprivation/recovery; RCD: regulated cell death; Z-VAD: Z-VAD-FMK.

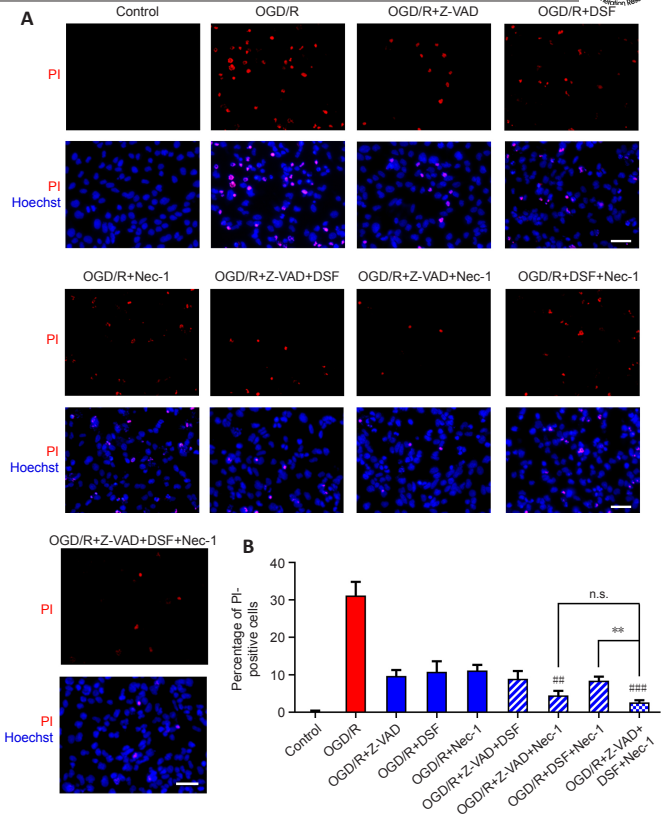

Figure 6 | Combination of RCD inhibitors decreases the OGD/R-induced PI-positive cells.
(A) PI staining for R28 cells treated with OGD/R and Z-VAD, DSF, and Nec-1. Red: PI-positive cells. Scale bars: 50 μm. (B) Percentage of PI-positive cells (mean ± SD, n = 3). **P < 0.01, *vs.* OGD/R + Z-VAD + DSF + Nec-1; ##P < 0.01, ###P < 0.001 *vs.* OGD/R+Nec-1 (Student's t-test). All cell experiments were performed at least three times independently. DSF: Disulfiram; n.s.: not significant; Nec-1: necrostatin-1; OGD/R: oxygen-glucose deprivation/recovery; PI: propidium iodide; RCD: regulated cell death; Z-VAD: Z-VAD-FMK.

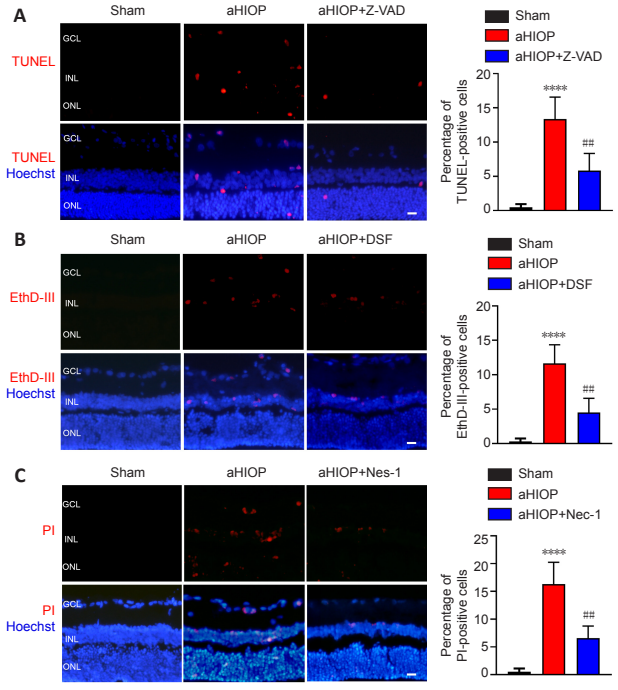

Figure 7 | aHIOP induces pyroptosis, apoptosis, and necroptosis *in vivo* in rat retina.
(A) TUNEL staining for rat retinal sections. The rats were treated with aHIOP and Z-VAD. (B) EthD-III staining for rat retinal sections. The rats were treated with aHIOP and DSF. (C) PI staining for rat retinal sections. The sections were treated with aHIOP and Nec-1. Scale bars: 50 μm. Percentage of TUNEL-, EthD-III-, and PI-positive cells shown to the right of images (mean ± SD, n = 5 rats per group). ***P < 0.001, *vs.* Sham; ##P < 0.01, *vs.* aHIOP (Student's t-test). aHIOP: Acute high intraocular pressure; DSF: disulfiram; GCL: ganglion cell layer; INL: inner nuclear layer; Nec-1: necrostatin-1; ONL: outer nuclear layer; Z-VAD: Z-VAD-FMK.

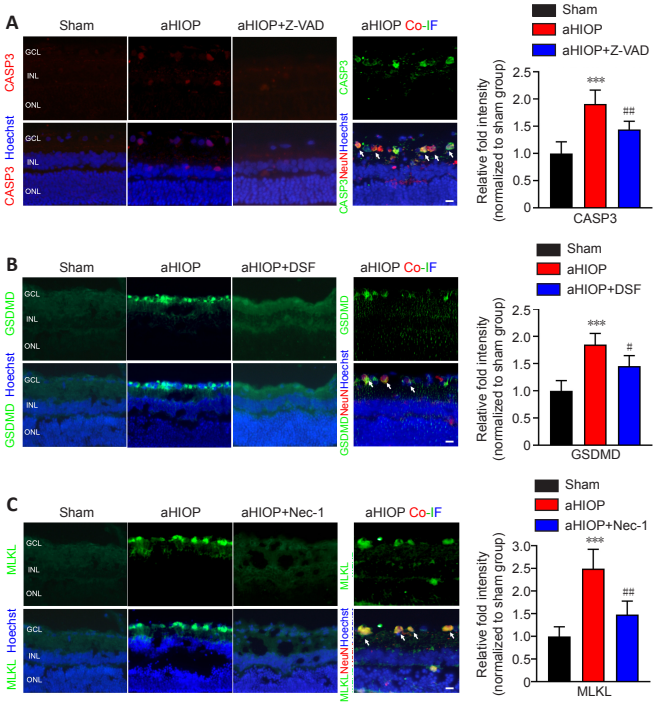

Figure 8 | aHIOP induces high expression of pyroptosis, apoptosis, and necroptosis-related proteins in rat retina.
Immunofluorescence staining of CASP3 (A), GSDMD (B) and MLKL (C) of rat retinal tissue sections. NeuN staining was used to indicate ganglion cells in the retina. Scale bars: 50 μm. Quantification of pyroptosis, apoptosis, and necroptosis-related protein expressions shown on the right of images (mean ± SD, n = 5 rats per group). Relative fold intensity of immunofluorescence staining was normalized relative to the intensity of the sham group. **P < 0.001, *vs.* Sham; #P < 0.05, ##P < 0.01, *vs.* OGD/R (Student's t-test). aHIOP: Acute high intraocular pressure; CASP: caspase; Co-IF: co-immunofluorescence; DSF: disulfiram; GCL: ganglion cell layer; GSDMD: gasdermin-D; INL: inner nuclear layer; Nec-1: necrostatin-1; MLKL: mixed lineage kinase domain-like; ONL: outer nuclear layer; Z-VAD: Z-VAD-FMK.

Discussion

Recent studies have indicated extensive crosstalk between RCD pathways, and PANoptosis is a newly defined phenomenon in which pyroptosis, apoptosis and necroptosis simultaneously occur in infectious disease, pathogen-induced immune response or inflammation (Malireddi et al., 2019). Furthermore, it has been shown that PANoptosis is regulated by the PANoptosome complex, which is composed of caspase-1, caspase-8, NLRP3, and other components (Christgen et al., 2020; Samir et al., 2020; Briard et al., 2021). Recent studies have indicated that the PANoptosome can be regulated by z-DNA binding protein 1 and TGF-β-activated kinase 1 to regulate the outcome of pyroptosis, apoptosis and necroptosis (Christgen et al., 2020; Samir et al., 2020). Findings from these studies suggested that identification and characterization of PANoptosis were vital to inform the development of targeted inhibitors for microbial infections and regulators of inflammatory cell death for therapeutic modulation of inflammation and the immune response. However, the existence of PANoptosis in noninfectious injuries and the nervous system remains unknown. Previous studies have established a process to investigate PANoptosis in disease or injury: the first level is to confirm the existence of PANoptosis-like cell death (simultaneous occurrence of pyroptosis, apoptosis and necroptosis). The second level is to study the existence of the PANoptosome that regulates the three RCDs simultaneously. And the third level is to find regulators of the PANoptosome. The main purpose of this study was to investigate whether PANoptosis-like cell death exists in nervous system I/R injury, and characterize the manifestation of PANoptosis-like cell death.

To investigate whether PANoptosis-like cell death plays a role in retinal I/R injury, R28 cells were selected for *in vitro* experimental study, and an OGD/R model was used to simulate I/R injury *in vitro*. Additionally, we selected Sprague Dawley rats for *in vivo* experiments, and used an aHIOP model to simulate *in vivo* I/R injury of retinal neurons. R28 cells are immortal retinal progenitor cells that are widely used to study retinal diseases and injuries (Huang et al., 2021). It is a classic cell line that simulates retinal neurons (Mathew et al., 2019, 2021). OGD/R and aHIOP models simulate I/R injury of retinal neurons (Osborne et al., 1995; Rosenbaum et al., 1998, 2001; Dvoriantchikova et al., 2010, 2014). They are widely used and generally accepted models at present (Rosenbaum et al., 1998, 2001; Dvoriantchikova et al., 2010).

Our experimental data showed that under the same model conditions and the same treatment time, pyroptosis, apoptosis and necroptosis occurred simultaneously after retinal I/R injury induced by OGD/R in R28 cells and aHIOP in rat retina. These data support the first level of the definition of PANoptosis, that is, PANoptosis-like cell death exists in retinal neuronal I/R injury. Previous studies on PANoptosis suggest that immune response and inflammatory response are closely related to the occurrence of PANoptosis (Kuriakose and Kanneganti, 2019; Banoth et al., 2020; Malireddi et al., 2020; Place et al., 2021). Similarly, studies on RCD of retinal neurons and other neurons have reported that the occurrence of pyroptosis is closely related to inflammatory factors (Homme et al., 2018; Zheng et al., 2019; Chen et al., 2020), and that key molecules of apoptosis can be regulated by inflammatory reactions (Toda and Nakanishi-Toda, 2007; Zheng et al., 2007; Cuenca et al., 2014). Necroptosis can also be initiated by inflammatory factors (Duprez et al., 2011; Kaczmarek et al., 2013; Liu et al., 2019a; Lin et al., 2020). The present study also showed that the protective effects of a combination of two inhibitors were not always better than those of a single inhibitor, indicating a potential crosstalk between those RCDs. Moreover, our results showed that pretreatment with three RCD inhibitors not only inhibited the kinase activity of death-signaling proteins to reduce the cell loss caused by I/R injury, but also significantly decreased the expression of those proteins in R28 cell clusters and rat retinal tissues. Without any intervention, expression of these proteins would increase in a signaling cascade affected by the release of inflammatory factors from surrounding cell death. Taken together, these findings suggest that the phenotypes and pathological mechanisms of cell death in retinal I/R injury have morphological features and pathological mechanisms in common with PANoptosis in infectious diseases.

This study preliminarily indicated the existence of PANoptosis-like cell death in I/R injury of retinal neurons, as observed by morphological features, protein levels, and the induction of important members of the PANoptosome (caspase-1, NLRP3, and RIPK3) under experimental conditions. Our previous literature mining research suggested that PANoptosis is likely to exist in nervous system diseases or injuries other than infectious diseases (Yan et al., 2022). The present study is only a beginning of PANoptosis-related research in retinal neurons, and does not address the wide range of the nervous system. Retinal precursor cells R28 do not fully represent brain tissue and the whole nervous system, although the retina is an important part of the central nervous system. Our results showed that the combination of all three inhibitors did not fully eliminate the cell loss induced by I/R injury, which suggests the existence of other signaling cascades or other types of RCD that could be involved in PANoptosis in this model. This study mainly focused on the first level study of PANoptosis to characterize the existence of PANoptosis-like cell death. In future experimental studies, it will be necessary to characterize the PANoptosome in I/R injury of retinal neurons, and to look for key molecules that regulate PANoptosis.

Author contributions: *Study conceptualization: KX and QZ; study design: KX, QZ, and WTY; study implementation: WTY and WJZ; data collection: WTY, WJZ, XMH, XXB, and WYN; manuscript writing: WTY and QZ; manuscript review and editing: KX, QZ, WTY, HW, and WJZ; study supervision: KX and QZ. All authors approved the final version of the manuscript.*
Conflicts of interest: *The authors declare that there is no potential conflict of interest.*
Editor note: KX is an editorial board member of Neural Regeneration Research. He was blinded from reviewing or making decisions on the manuscript. The article was subject to the journal's standard procedures, with peer review handled independently of this Editorial Board member and their research groups.

References

Banoth B, Tuladhar S, Karki R, Sharma BR, Briard B, Kesavardhana S, Burton A, Kanneganti TD (2020) ZBP1 promotes fungi-induced inflammasome activation and pyroptosis, apoptosis, and necroptosis (PANoptosis). J Biol Chem 295:18276-18283.

Basuroy S, Bhattacharya S, Leffler CW, Parfenova H (2009) Nox4 NADPH oxidase mediates oxidative stress and apoptosis caused by TNF-alpha in cerebral vascular endothelial cells. Am J Physiol Cell Physiol 296:C422-432.

Briard B, Malireddi RKS, Kanneganti TD (2021) Role of inflammasomes/pyroptosis and PANoptosis during fungal infection. PLoS Pathog 17:e1009358.

Chen H, Deng Y, Gan X, Li Y, Huang W, Lu L, Wei L, Su L, Luo J, Zou B, Hong Y, Cao Y, Liu Y, Chi W (2020) NLRP12 collaborates with NLRP3 and NLRC4 to promote pyroptosis inducing ganglion cell death of acute glaucoma. Mol Neurodegener 15:26.

Chen S, Yan J, Deng HX, Long LL, Hu YJ, Wang M, Shang L, Chen D, Huang JF, Xiong K (2016) Inhibition of calpain on oxygen glucose deprivation-induced RGC-5 necroptosis. J Huazhong Univ Sci Technolog Med Sci 36:639-645.

Chen Y, Li Y, Guo L, Hong J, Zhao W, Hu X, Chang C, Liu W, Xiong K (2021) Bibliometric analysis of the inflammasome and pyroptosis in brain. Front Pharmacol 11:626502.

Christgen S, Zheng M, Kesavardhana S, Karki R, Malireddi RKS, Banoth B, Place DE, Briard B, Sharma BR, Tuladhar S, Samir P, Burton A, Kanneganti TD (2020) Identification of the PANoptosome: A molecular platform triggering pyroptosis, apoptosis, and necroptosis (PANoptosis). Front Cell Infect Microbiol 10:237.

Cuenca N, Fernández-Sánchez L, Campello L, Maneu V, De la Villa P, Lax P, Pinilla I (2014) Cellular responses following retinal injuries and therapeutic approaches for neurodegenerative diseases. Prog Retin Eye Res 43:17-75.

Degterev A, Hitomi J, Germscheid M, Ch'en IL, Korkina O, Teng X, Abbott D, Cuny GD, Yuan C, Wagner G, Hedrick SM, Gerber SA, Lugovskoy A, Yuan J (2008) Identification of RIP1 kinase as a specific cellular target of necrostatins. Nat Chem Biol 4:313-321.

Duprez L, Takahashi N, Van Hauwermeiren F, Vandendriessche B, Goossens V, Vanden Berghe T, Declercq W, Libert C, Cauwels A, Vandenabeele P (2011) RIP kinase-dependent necrosis drives lethal systemic inflammatory response syndrome. Immunity 35:908-918.

Dvoriantchikova G, Barakat DJ, Hernandez E, Shestopalov VI, Ivanov D (2010) Liposome-delivered ATP effectively protects the retina against ischemia-reperfusion injury. Mol Vis 16:2882-2890.

Dvoriantchikova G, Degterev A, Ivanov D (2014) Retinal ganglion cell (RGC) programmed necrosis contributes to ischemia-reperfusion-induced retinal damage. Exp Eye Res 123:1-7.

Elmore S (2007) Apoptosis: A review of programmed cell death. Toxicol Pathol 35:495-516.

Ge XT, Li WZ, Huang S, Yin ZY, Xu X, Chen FL, Kong XD, Wang HC, Zhang JN, Lei P (2018) The pathological role of NLRs and AIM2 inflammasome-mediated pyroptosis in damaged blood-brain barrier after traumatic brain injury. Brain Res 1697:10-20.

Guo LM, Wang Z, Li SP, Wang M, Yan WT, Liu FX, Wang CD, Zhang XD, Chen D, Yan J, Xiong K (2020) RIP3/MLKL-mediated neuronal necroptosis induced by methamphetamine at 39°C. Neural Regen Res 15:865-874.

Homme RP, Singh M, Majumder A, George AK, Nair K, Sandhu HS, Tyagi N, Lominadze D, Tyagi SC (2018) Remodeling of retinal architecture in diabetic retinopathy: disruption of ocular physiology and visual functions by inflammatory gene products and pyroptosis. Front Physiol 9:1268.

Hu JJ, Liu X, Xia S, Zhang Z, Zhang Y, Zhao J, Ruan J, Luo X, Lou X, Bai Y, Wang J, Hollingsworth LR, Magupalli VG, Zhao L, Luo HR, Kim J, Lieberman J, Wu H (2020a) FDA-approved disulfiram inhibits pyroptosis by blocking gasdermin D pore formation. Nat Immunol 21:736-745.

Hu XM, Li ZX, Lin RH, Shan JQ, Yu QW, Wang RX, Liao LS, Yan WT, Wang Z, Shang L, Huang Y, Zhang Q, Xiong K (2021) Guidelines for regulated cell death assays: a systematic summary, a categorical comparison, a prospective. Front Cell Dev Biol 9:634690.

Hu YD, Tang CL, Jiang JZ, Lv HY, Wu YB, Qin XD, Shi S, Zhao B, Zhu XN, Xia ZY (2020b) Neuroprotective effects of dexmedetomidine preconditioning on oxygen-glucose deprivation-reoxygenation injury in PC12 cells via regulation of Ca(2+)-STIM1/Orai1 signaling. Curr Med Sci 40:699-707.

Huang JF, Shang L, Zhang MQ, Wang H, Chen D, Tong JB, Huang H, Yan XX, Zeng LP, Xiong K (2013) Differential neuronal expression of receptor interacting protein 3 in rat retina: involvement in ischemic stress response. BMC Neurosci 14:16.

Huang Y, Wang S, Huang F, Zhang Q, Qin B, Liao L, Wang M, Wan H, Yan W, Chen D, Liu F, Jiang B, Ji D, Xia X, Huang J, Xiong K (2021) c-FLIP regulates pyroptosis in retinal neurons following oxygen-glucose deprivation/recovery via a GSDMD-mediated pathway. Ann Anat 235:151672.

Huang Z, Zhou T, Sun X, Zheng Y, Cheng B, Li M, Liu X, He C (2018) Necroptosis in microglia contributes to neuroinflammation and retinal degeneration through TLR4 activation. Cell Death Differ 25:180-189.

Kaczmarek A, Vandenabeele P, Krysko DV (2013) Necroptosis: the release of damage-associated molecular patterns and its physiological relevance. Immunity 38:209-223.

Karki R, Sharma BR, Tuladhar S, Williams EP, Zalduondo L, Samir P, Zheng M, Sundaram B, Banoth B, Malireddi RKS, Schreiner P, Neale G, Vogel P, Webby R, Jonsson CB, Kanneganti TD (2021) Synergism of TNF-α and IFN-γ triggers inflammatory cell death, tissue damage, and mortality in SARS-CoV-2 infection and cytokine shock syndromes. Cell 184:149-168.e17.

Kesavardhana S, Kanneganti TD (2017) Mechanisms governing inflammasome activation, assembly and pyroptosis induction. Int Immunol 29:201-210.

Kuriakose T, Kanneganti TD (2019) Pyroptosis in antiviral immunity. Curr Top Microbiol doi:10.1007/82_2019_189.

Liao LS, Lu S, Yan WT, Wang SC, Guo LM, Yang YD, Huang K, Hu XM, Zhang Q, Yan J, Xiong K (2021) The role of HSP90α in methamphetamine/hyperthermia-induced necroptosis in rat striatal neurons. Front Pharmacol 12:716394.

Lin Y, Yu M, Fan T (2020) Insights into mechanisms of pranoprofen-induced apoptosis and necroptosis in human corneal stromal cells. Toxicol Lett 320:9-18.

Liu W, Xia F, Ha Y, Zhu S, Li Y, Folorunso O, Pashaei-Marandi A, Lin PY, Tilton RG, Pierce AP, Liu H, Zhang W (2019a) Neuroprotective effects of HSF1 in retinal ischemia-reperfusion injury. Invest Ophthalmol Vis Sci 60:965-977.

Liu Y, Liu T, Lei T, Zhang D, Du S, Girani L, Qi D, Lin C, Tong R, Wang Y (2019b) RIP1/RIP3-regulated necroptosis as a target for multifaceted disease therapy (Review). Int J Mol Med 44:771-786.

Malireddi RKS, Kesavardhana S, Kanneganti TD (2019) ZBP1 and TAK1: master regulators of NLRP3 inflammasome/pyroptosis, apoptosis, and necroptosis (PAN-optosis). Front Cell Infect Microbiol 9:406.

Malireddi RKS, Gurung P, Kesavardhana S, Samir P, Burton A, Mummareddy H, Vogel P, Pelletier S, Burgula S, Kanneganti TD (2020) Innate immune priming in the absence of TAK1 drives RIPK1 kinase activity-independent pyroptosis, apoptosis, necroptosis, and inflammatory disease. J Exp Med 217.

Mathew B, Ravindran S, Liu X, Torres L, Chennakesavalu M, Huang C-C, Feng L, Zelka R, Lopez J, Sharma M, Roth S (2019) Mesenchymal stem cell-derived extracellular vesicles and retinal ischemia-reperfusion. Biomaterials 197:146-160.

Mathew B, Chennakesavalu M, Sharma M, Torres LA, Stelman CR, Tran S, Patel R, Burg N, Salkovski M, Kadzielawa K, Seiler F, Aldrich LN, Roth S (2021) Autophagy and post-ischemic conditioning in retinal ischemia. Autophagy 17:1479-1499.

McKenzie BA, Dixit VM, Power C (2020) Fiery cell death: pyroptosis in the central nervous system. Trends Neurosci 43:55-73.

Nicoletti I, Migliorati G, Pagliacci MC, Grignani F, Riccardi C (1991) A rapid and simple method for measuring thymocyte apoptosis by propidium iodide staining and flow cytometry. J Immunol Methods 139:271-279.

Ofengeim D, Ito Y, Najafov A, Zhang YY, Shan B, DeWitt JP, Ye JY, Zhang XM, Chang AS, Vakifahmetoglu-Norberg H, Geng JF, Py B, Zhou W, Amin P, Lima JB, Qi CT, Yu Q, Trapp B, Yuan JY (2015) Activation of necroptosis in multiple sclerosis. Cell Reports 10:1836-1849.

Osborne NN, Larsen A, Barnett NL (1995) Influence of excitatory amino acids and ischemia on rat retinal choline acetyltransferase-containing cells. Invest Ophthalmol Vis Sci 36:1692-1700.

Pan J, Han L, Guo J, Wang X, Liu D, Tian J, Zhang M, An F (2018) AIM2 accelerates the atherosclerotic plaque progressions in ApoE-/- mice. Biochem Biophys Res Commun 498:487-494.

Pasparakis M, Vandenabeele P (2015) Necroptosis and its role in inflammation. Nature 517:311-320.

Place DE, Lee S, Kanneganti TD (2021) PANoptosis in microbial infection. Curr Opin Microbiol 59:42-49.

Quigley HA, Nickells RW, Kerrigan LA, Pease ME, Thibault DJ, Zack DJ (1995) Retinal ganglion cell death in experimental glaucoma and after axotomy occurs by apoptosis. Invest Ophthalmol Vis Sci 36:774-786.

Riccardi C, Nicoletti I (2006) Analysis of apoptosis by propidium iodide staining and flow cytometry. Nat Protoc 1:1458-1461.

Rong R, Xia X, Peng H, Li H, You M, Liang Z, Yao F, Yao X, Xiong K, Huang J, Zhou R, Ji D (2020) Cdk5-mediated Drp1 phosphorylation drives mitochondrial defects and neuronal apoptosis in radiation-induced optic neuropathy. Cell Death Dis 11:720.

Rosenbaum DM, Rosenbaum PS, Singh M, Gupta G, Gupta H, Li B, Roth S (2001) Functional and morphologic comparison of two methods to produce transient retinal ischemia in the rat. J Neuroophthalmol 21:62-68.

Rosenbaum DM, Rosenbaum PS, Gupta H, Singh M, Aggarwal A, Hall DH, Roth S, Kessler JA (1998) The role of the p53 protein in the selective vulnerability of the inner retina to transient ischemia. Invest Ophthalmol Vis Sci 39:2132-2139.

Samir P, Malireddi RKS, Kanneganti TD (2020) The PANoptosome: a deadly protein complex driving pyroptosis, apoptosis, and necroptosis (PANoptosis). Front Cell Infect Microbiol 10:238.

Saraste A, Pulkki K (2000) Morphologic and biochemical hallmarks of apoptosis. Cardiovasc Res 45:528-537.

Semmler A, Okulla T, Sastre M, Dumitrescu-Ozimek L, Heneka MT (2005) Systemic inflammation induces apoptosis with variable vulnerability of different brain regions. J Chem Neuroanat 30(2-3):144-157.

Shimizu T, Pommier Y (1997) Camptothecin-induced apoptosis in p53-null human leukemia HL60 cells and their isolated nuclei: effects of the protease inhibitors Z-VAD-fmk and dichloroisocoumarin suggest an involvement of both caspases and serine proteases. Leukemia 11:1238-1244.

Slee EA, Zhu H, Chow SC, MacFarlane M, Nicholson DW, Cohen GM (1996) Benzyloxycarbonyl-Val-Ala-Asp (OMe) fluoromethylketone (Z-VAD.FMK) inhibits apoptosis by blocking the processing of CPP32. Biochem J 315 (Pt 1):21-24.

Takeda K, Noguchi T, Naguro I, Ichijo H (2008) Apoptosis signal-regulating kinase 1 in stress and immune response. Annu Rev Pharmacol Toxicol 48:199-225.

Tan MS, Tan L, Jiang T, Zhu XC, Wang HF, Jia CD, Yu JT (2014) Amyloid-beta induces NLRP1-dependent neuronal pyroptosis in models of Alzheimer's disease. Cell Death Dis 5:12.

Toda N, Nakanishi-Toda M (2007) Nitric oxide: ocular blood flow, glaucoma, and diabetic retinopathy. Prog Retin Eye Res 26:205-238.

Van Noorden CJF (2001) The history of Z-VAD-FMK, a tool for understanding the significance of caspase inhibition. Acta Histochem103:241-251.

Vandenabeele P, Galluzzi L, Vanden Berghe T, Kroemer G (2010) Molecular mechanisms of necroptosis: an ordered cellular explosion. Nat Rev Mol Cell Biol 11:700-714.

Wang M, Wan H, Wang S, Liao L, Huang Y, Guo L, Liu F, Shang L, Huang J, Ji D, Xia X, Jiang B, Chen D, Xiong K (2020) RSK3 mediates necroptosis by regulating phosphorylation of RIP3 in rat retinal ganglion cells. J Anat 237:29-47.

Wang S, Huang Y, Yan Y, Zhou H, Wang M, Liao L, Wang Z, Chen D, Ji D, Xia X, Liu F, Huang J, Xiong K (2019a) Calpain2 but not calpain1 mediated by calpastatin following glutamate-induced regulated necrosis in rat retinal neurons. Ann Anat 221:57-67.

Wang X, Pan J, Liu H, Zhang M, Liu D, Lu L, Tian J, Liu M, Jin T, An F (2019b) AIM2 gene silencing attenuates diabetic cardiomyopathy in type 2 diabetic rat model. Life Sci 221:249-258.

Wang Z, Guo LM, Wang Y, Zhou HK, Wang SC, Chen D, Huang JF, Xiong K (2018) Inhibition of HSP90α protects cultured neurons from oxygen-glucose deprivation induced necroptosis by decreasing RIP3 expression. J Cell Physiol 233:4864-4884.

Wu X, Hu X, Zhang Q, Liu F, Xiong K (2021) Regulatory role of chinese herbal medicine in regulated neuronal death. CNS Neurol Disord Drug Targets 20:228-248.

Xie P, Ren ZK, Lv J, Hu YM, Guan ZZ, Yu WF (2020) Berberine ameliorates oxygen-glucose deprivation/reperfusion-induced apoptosis by inhibiting endoplasmic reticulum stress and autophagy in PC12 cells. Curr Med Sci 40:1047-1056.

Yan WT, Yang YD, Hu XM, Ning WY, Liao LS, Lu S, Zhao WJ, Zhang Q, Xiong K (2022) Do pyroptosis, apoptosis, and necroptosis (PANoptosis) exist in cerebral ischemia? Evidence from cell and rodent studies. Neural Regen Res 17:1761-1768.

Yan WT, Lu S, Yang YD, Ning WY, Cai Y, Hu XM, Zhang Q, Xiong K (2021) Research trends, hot spots and prospects for necroptosis in the field of neuroscience. Neural Regen Res 16:1628-1637.

Yuan JY, Yankner BA (2000) Apoptosis in the nervous system. Nature 407:802-809.

Yuan JY, Amin P, Ofengeim D (2019) Necroptosis and RIPK1-mediated neuroinflammation in CNS diseases. Nat Rev Neurosci 20:19-33.

Zhang J, Dai Y, Yang Y, Xu J (2021a) Calcitriol alleviates hyperosmotic stress-induced corneal epithelial cell damage via inhibiting the NLRP3-ASC-Caspase-1-GSDMD pyroptosis pathway in dry eye disease. J Inflamm Res 14:2955-2962.

Zhang Y, Zhang R, Han X (2021b) Disulfiram inhibits inflammation and fibrosis in a rat unilateral ureteral obstruction model by inhibiting gasdermin D cleavage and pyroptosis. Inflamm Res 70:543-552.

Zheng L, Gong B, Hatala DA, Kern TS (2007) Retinal ischemia and reperfusion causes capillary degeneration: Similarities to diabetes. Invest Ophthalmol Vis Sci 48:361-367.

Zheng Q, Zou H, Gao L, Chen K, Liu W, Ji S, Chu X, Yuan R, Ye J (2019) The levels and significance of inflammasomes in the mouse retina following optic nerve crush. Int Immunopharmacol 71:313-320.

Zhou Y, Gu Y, Liu J (2019) BRD4 suppression alleviates cerebral ischemia-induced brain injury by blocking glial activation via the inhibition of inflammatory response and pyroptosis. Biochem Biophys Res Commun 519:481-488.

C-Editor: Zhao M; S-Editor: Li CH; L-Editors: McCollum L, Song LP; T-Editor: Jia Y